RSC Advances

PAPER

View Article Online
View Journal | View Issue

Cite this: *RSC Adv.*, 2025, **15**, 35971

Eco-benign spectrofluorimetric analysis of icariin in a nano-formulation using green quantum dots: insights from *in vitro* anticoagulant and docking studies

Haydi S. Elbordiny, *[a] Aya R. Ahmed, [b] Mai M. Elnaggar,[b] Mona M. Agwa,[c] Mahmoud A. Ragab[a] and Sara I. Aboras[b]

The analysis of nutraceuticals is crucial for assessing their safety, efficacy, and bioavailability and helps in their effective integration into health practices. Icariin (ICA), a natural flavonoid, was analyzed *via* a selective and sensitive method using a microwave-synthesized turn-off fluorescence probe. Full characterization of the probe was performed using several techniques. It was observed that fluorescence quenching was directly proportional to the increase in ICA concentration over a range of 1–20 μg mL^{-1} with a linearity correlation coefficient of 0.9998. Additionally, the estimated values for the limits of detection and quantitation were 0.24 and 0.73 μg mL^{-1}, respectively. Growing interest in ICA's potential to prevent and/or treat diseases with fewer side effects and better bioavailability has highlighted the need for innovative new nano-formulations. ICA was encapsulated in a milk-based nano-formulation and tested *in vitro* for its anticoagulant activity, employing both extrinsic and intrinsic coagulation mechanisms. Additionally, *in vitro* blood hemolysis was accomplished to certify its suitability for further *in vivo* application. The outcomes of the *in vitro* anticoagulant assays were affirmed by a molecular docking study of ICA with different coagulation factors. Finally, the trio color-coded assessment of the method using versatile tools was implemented and juxtaposed with other reported analytical techniques for the assay of ICA. Additionally, the devised method's compatibility with the Sustainable Development Goals (SDGs) was demonstrated. This work offers a straightforward, cost-effective, sensitive methodology for the assay of ICA in nano-formulations. It gives insights into the crucial role of ICA as a prophylactic anticoagulant nutraceutical.

Received 7th July 2025
Accepted 11th September 2025

DOI: 10.1039/d5ra04854k

rsc.li/rsc-advances

1 Introduction

Cardiovascular diseases (CVDs) symbolize one of the most prominent health issues. Heart attacks and strokes often lead to mortal outcomes, the main underlying issue being thrombus generation, which can block vessels and hamper the normal blood flow.[1] Several prophylactic therapeutic approaches involving warfarin and acetylsalicylic acid are recommended to avoid thrombotic complications among patients with cardiovascular diseases.[2] However, long-term administration of these drugs is prone to cause toxic effects, including gastrointestinal abnormalities caused by acetylsalicylic acid and hemorrhagic risk caused by warfarin.[3] Thus, discovering new therapeutics of plant origin, particularly those that are rich in flavonoids, is of interest to prevent thrombus generation.[4,5] Previous studies have certified that including flavonoids in the diet is linked to a lower risk of cardiovascular and thrombotic disorders.[6,7]

Icariin (ICA) (Fig. 1A) is a flavonol glycoside and is considered the active moiety of the *Epimedium* species. For many years in traditional Chinese medicine (TCM), the *Epimedium* species (aka horny goat weed) have been used for erectile dysfunction treatment. ICA is also renowned for its pharmacological effects, such as neuroprotective, anti-inflammatory, anticancer, antioxidant, hypoglycemic, immunomodulatory, and osteogenic properties.[8] Additionally, ICA has displayed a wide range of cardiovascular protective properties *via* ameliorating oxidative stress and inflammation reactions, organizing cellular propagation and apoptosis, and suppressing vascular endothelial cell damages.[9,10] However, certain restrictions have been brought about due to the characteristics and method of administration of either ICA or its metabolites. Firstly, oral administration is not appropriate for ICA as it requires great permeability and solubility, which this nutraceutical lacks.[11] Furthermore, there

[a]*Department of Pharmaceutical Chemistry, Faculty of Pharmacy, Damanhour University, Damanhour, Egypt. E-mail: Haydi.elbordiny@pharm.dmu.edu.eg*
[b]*Department of Pharmaceutical Analytical Chemistry, Faculty of Pharmacy, Alexandria University, Alexandria, Egypt*
[c]*Department of Chemistry of Natural and Microbial Products, Pharmaceutical and Drug Industries Research Institute, National Research Centre, 33 El-Behooth St, Dokki, Giza 12622, Egypt*

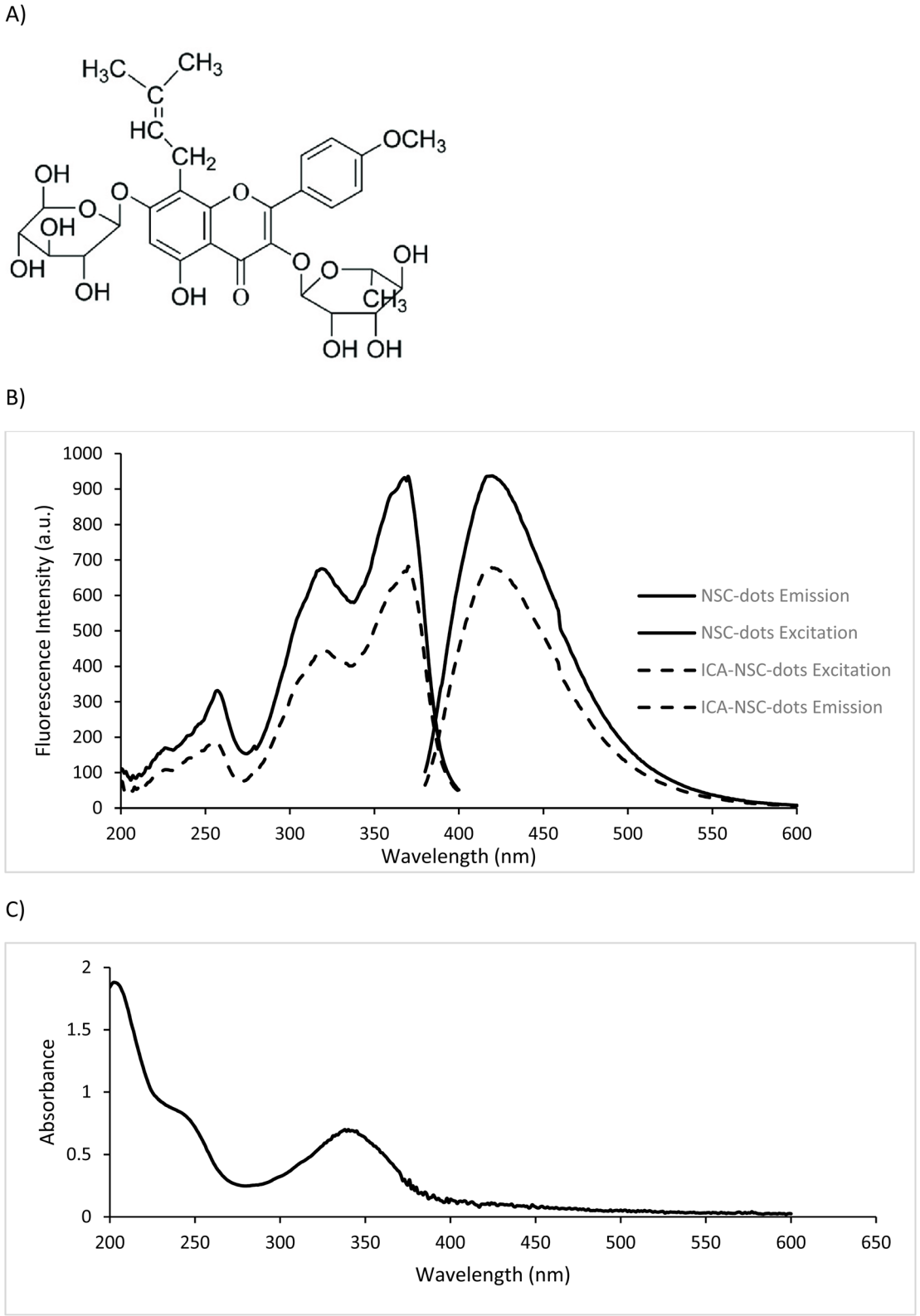

Fig. 1 (A) Chemical structure of icariin (ICA). (B) Excitation and emission spectra of NSC-dots in the absence (solid line) and presence (dotted line) of 20 μg mL^{-1} of ICA (λ emission = 418 nm and λ excitation = 370 nm). (C) Absorption spectra of NSC-dots.

are some challenges associated with the oral administration of ICA, such as its instability in the luminal fluid, insolubility in the digestive tract, inadequate absorption in the mucosal membrane and cell membrane, and loss of bioactivity following the initial pass drug elimination process.[12] Nevertheless, the ICA's anticoagulant properties have not yet been investigated.

The improvement of ICA's chemical instability and/or poor bioavailability has been a workable way to enhance therapeutic outcomes. The utilization of nanotechnology *via* harnessing natural drug carriers is a feasible strategy for resolving these problems and enhancing the therapeutic potential of ICA owing to their outstanding biocompatibility, biodegradability, and remarkable safety.[13–17]

To the best of our knowledge, no previous fluorometric analytical method has been reported for ICA, although HPLC in tandem with a UV[18–20] or MS/MS detector[21,22] is widely used for the quantitative determination of icariin due to its sensitivity and specificity. Capillary zone electrophoresis (CZE)[23,24] and HPTLC[25] methods have also been developed for icariin analysis.[23]

Carbon dots, or CDs, have attracted a lot of interest lately because of their excellent photostability, ease of synthesis, low cost, and exceptional biocompatibility. These materials range in size from 2 to 10 nm, making them a kind of nanomaterial. Many studies have focused on surface functionalization or heteroatom doping to improve the CDs' optical, chemical, and electrical properties.[26,27] Single-atom or multi-atom doping of CDs can be employed, depending on the number of doped heteroatoms; the latter is recommended since the doped heteroatoms cooperate to produce unique electronic structures.[27–30] Nitrogen and sulfur are the heteroatoms that are most frequently used to dope CDs. Their strong valence bond, similar atomic size (N:0.75, C:0.77), and similar electronegativity (C:2.55, S:2.58) allow them to potentially produce new active sites, extra defective sites, and electron pairs, which might alter the chemical activity of carbon nanoparticles.[26,31] Doped CDs have proved to be useful for several applications, including bioimaging, sensors, catalysis, and medicine delivery.[26,27,32]

On the other hand, metal-based QDs (*e.g.*, CdSe, CdTe, and PbS) offer superior optical performance, with high quantum yields and narrow emission spectra, driving their widespread use in biomedical imaging.[33] However, their heavy-metal content poses toxicity and environmental risks, and regulatory restrictions often limit their pharmaceutical and clinical applications.[34]

In contrast, CDs offer a slight reduction in quantum yield in exchange for exceptional biocompatibility, low toxicity, and sustainability. Composed mainly of carbon, they avoid heavy-metal hazards while providing safer, greener, and regulatory-compliant alternatives for biomedical use.[35]

Leveraging their unique photophysical properties, carbon dots (CDs) are gaining considerable attention as a superior alternative to traditional organic fluorophores.[36] While numerous methods exist for assaying icariin (ICA), this study presents a novel, eco-friendly, and highly sensitive spectrofluorimetric method for its determination. This approach is based on a unique "turn-off" fluorescence sensing platform where CDs act as a green, biocompatible probe that is selectively quenched by ICA.

In addition to developing this analytical procedure, we successfully used the system to quantify ICA in a novel whey protein-based nano-formulation. This formulation enhanced ICA's bioavailability and was designed to explore its potential as a safer, prophylactic alternative to traditional anticoagulant drugs. The anticoagulant activity was further validated through a molecular docking study. This work's primary contribution lies in its dual focus: introducing a simple and sensitive analytical procedure for ICA using quantum dots while also underscoring the crucial, previously unexplored role of ICA as an anticoagulant nutraceutical.

2 Experimental

2.1. Chemicals and reagents

Icariin (ICA) (purity >98% ± 1%) was purchased from Medchemexpress, USA, while the whey protein concentrate from bovine milk was bought from Sigma-Aldrich (St. Louis, USA). Solvents and reagents, such as methanol, ethanol, isopropanol, acetone, acetonitrile, hydrochloric acid, phosphoric acid, sulphuric acid, sodium bicarbonate, sodium hydroxide, boric acid, and glacial acetic acid, were mostly supplied by the El Nasr Chemical Company, Cairo, Egypt. L-Cysteine, the main constituent in quantum dots, with a purity of 98%, and anhydrous citric acid, with a purity of 99%, were shipped out from Loba Chemie, Mumbai, India. The diluent (water) used for the entire trial was deionized daily.

2.2. Animals

Eight Wistar male rats weighing between 200 and 260 grams were provided for our experimental study by the Laboratory Animal Centre of the Alexandria University Faculty of Pharmacy. The rats were kept in an acoustically regulated metabolic cage with a temperature and relative humidity maintained at 25 ± 2 °C and 45–55% rh, respectively, before the start point of the experiment. Throughout the study, they were supplied with standard laboratory fare and water. The animal trials were approved by the Faculty of Pharmacy's Care and Use of Animals Committee (Ethical Approval Number: AU0620247293242).

2.3. Instruments and software

Spectrofluorometric readings were taken using a Cary Eclipse fluorescence spectrophotometer (Agilent Technologies, USA; model: G9800A). The synthesis of the QDs was carried out using a domestic microwave oven (Daewoo model: KOG-1B5H). QDs were characterized using a Shimadzu UV-vis light spectrophotometer (USA model 1800), an Agilent Cary 360 Fourier transform infrared spectrometer and a Thermo Scientific K Alpha X-ray photoelectron spectrometer to assess their chemical composition. Furthermore, the crystalline structure of the synthesized NSC dots was investigated by a TEM-1400 plus electron microscope. The *in vitro* anticoagulant assay harnessing prothrombin time (PT) and activated partial thromboplastin time (aPTT) was performed using an automated coagulometer (MC 4, Merlin, Germany). Prism8.0.1; GraphPad (San Diego, CA, USA) was used for the statistical analysis of the data. Finally, the software adopted for the *in silico* docking inquiry was Flare™, version 9.0, Cresset® (Litlington, Cambridgeshire, UK).

2.4. Microwave-driven quantum dots synthesis

A mass of 0.91 g of anhydrous citric acid (4.75 mmol) and 0.5 g L-cysteine (4.15 mmol) was dissolved in 5 mL of deionized water, in a round-bottomed plug-sealed Pyrex tube (15 mL). The mixture was heated in a microwave for 3.5 minutes at 1000 W in the household microwave oven. Afterwards, the reaction mixture was cooled down to room temperature. The resultant black syrup was neutralized using a 1 M sodium bicarbonate solution, diluted to 50 mL with deionized water, and ultrasonically agitated for 5 minutes at room temperature before the final filtration step.

2.4.1. Purification protocol. Following the hydrothermal synthesis and neutralization steps, the crude NSC dots solution underwent purification using a dialysis membrane with 1000 Da molecular weight cut-off (MWCO) for 48 hours against deionized water. The dialysis process was conducted with regular water changes every 8 hours to ensure complete removal of the unreacted precursors, salt byproducts, and other small molecular impurities.

This purification step is critical for obtaining high-purity NSC dots and ensuring accurate characterization results, particularly for quantum yield measurements and spectroscopic analyses. The 1000 Da MWCO was selected to retain the carbon dots while effectively removing low molecular weight impurities, including unreacted citric acid, L-cysteine, and sodium salts formed during the neutralization process.

2.5. Stock solution preparation and construction of the calibration curve

An accurate weight of ICA powder was dissolved in methanol to prepare a 1000 μg mL^{-1} stock solution. Then, various aliquots of ICA stock solution in addition to the standard volume of the NSC-dots reagent (0.1 mL) were transferred into a set of 10-mL volumetric flasks and diluted with deionized water to cover the nominated concentration range (1–20 μg mL^{-1}). The change in the fluorescence intensity of the working solutions was tracked at λ emission = 418 nm (λ excitation = 370 nm). Each measurement was deducted from the blank reading, which underwent the identical procedure. The calibration graph was obtained by plotting the subtraction in fluorescence intensity *versus* the appropriate concentrations of ICA.

2.6. Preparation of icariin-incorporated nanocarriers

The nano-delivery system comprising ICA-loaded whey protein nanoparticles was prepared *via* the solvent evaporation method.[37–39] Briefly, 10 mg of ICA was fully dissolved in an appropriate volume of methanol and then added dropwise to an aqueous whey solution (100 mg/10 mL) under stirring, and this was left at ambient temperature for 24 h until complete methanol evaporation was achieved. The prepared drug-incorporated nanoparticles were subjected to lyophilization, and the attained nanoparticle powder was preserved for further experiments involving measuring the size, zeta potential, encapsulation efficiency, and assessing the *in vitro* anticoagulant potential, along with the hemolysis test.

The suggested fluorometric approach was used to evaluate the amount of free ICA in order to determine the entrapment efficiency, as stated in the previous study.[40] By comparing the computed value with the nominally added one, the overall ICA content assay (% recovery) of the formula was evaluated. The following eqn (1) was used to elaborate the entrapment efficiency (EE):[41,42]

$$\%\ \mathrm{EE} = \frac{\text{amount of ICA entrapped in nanoformulation}}{\text{the initial amount of ICA in nanoformulation}} \times 100 \quad (1)$$

2.7. *In vitro* blood hemolysis

The hemolytic percentages of ICA-loaded whey nanoparticles were checked by quantifying the released haemoglobin from erythrocytes after incubation with red blood cells (RBCs). Blood from healthy rats was collected in EDTA tubes and instantly centrifuged for 5 minutes at 700×*g*. The collected RBCs were washed with saline (0.9% NaCl) and then diluted to obtain a 0.1% RBC suspension after abolishing the upper plasma layer. A 500-μL volume of the prepared 0.1% erythrocyte suspension was incubated with 500 μL of different concentrations of the test compound (0.1–2 mg mL^{-1}) for 60 minutes at 37 °C under 100 rpm shaking using Triton X-100 as a positive control and saline as a negative control. After incubation, the samples were centrifuged for 10 minutes at 7000×*g*, and the released hemoglobin was assessed spectrophotometrically at 545 nm; then the percentage was quantified as follows.[39,43]

$$\%\ \text{Hemoglobin release} = \frac{\mathrm{Ab(sample)} - \mathrm{Ab(negative\ control)}}{\mathrm{Ab(positive\ control)} - \mathrm{Ab(negative\ control)}} \times 100 \quad (2)$$

2.8. Anticoagulation potential assay

The anticoagulation potential assay of the ICA-incorporated whey nanocarriers and whey nanoparticles was conducted by measuring the prothrombin time (PT) and activated partial thromboplastin time (aPTT) to determine the clotting time, using an automated coagulometer (MC 4, Merlin, Germany).[44,45] All tested samples involving whey nanoparticles (40 mg mL^{-1}) and ICA-incorporated whey nanocarriers (40 mg mL^{-1} whey; 2 mg mL^{-1} icariin) were dissolved in normal saline. The tested samples were replaced with normal saline as a negative control. In the assay, fresh blood was drained from normal rats in citrated tubes and then centrifuged at 4000 rpm under cooling for 20 minutes to obtain the plasma for the experiment. In the PT assay, disconnected plasma (30 μl) was incubated with the tested sample (20 μl) for 3 minutes at 37 °C, then added to 100 μl of the pre-incubated PT reagent at 37 °C, recording the clotting time. In an aPTT assay, disconnected plasma (30 μl) was incubated with the tested sample (20 μl) for 3 minutes at 37 °C, then incubated with 50 μL aPTT reagent at 37 °C for 3 minutes. About 50 μL of 0.025 mol L^{-1} $CaCl_2$ solution that had been previously incubated for 3 minutes at 37 °C was added, followed by recording the clotting time.

One-way analysis of variance (ANOVA) was used to compute the mean ± standard deviation (SD) of all collected data in the

presence and absence of ICA and whey nanoparticles. Tukey's post hoc analysis was then performed to determine the statistical significance at $p < 0.05$ (Prism8.0.1; GraphPad, San Diego, CA, USA).

2.9. *In silico* studies

Crystal structures for coagulation factors Xa (PDB: 1IGQ), IXa (PDB: 3LC3), XIa (PDB: 4TY6) and XIIa (PDB: 6B74) were downloaded from the protein databank website and used for a molecular docking study. Preparation of the crystal structures was performed using the Protein Preparation Wizard tool implemented in Flare 9.0.0 suite to add hydrogens, delete non-structural water molecules, assign the protonation state for the ionizable amino acids and ligand groups, and optimize the H-bonding networks. The energy minimization was performed using the Flare energy minimize wizard using Accurate XED calculations.

Docking was performed using the Lead Finder docking algorithm implemented in Flare 9.0.0 by using the "Very Accurate but Slow" method and by centering a 7.0 Å docking grid on the crystallographic ligands. In both cases, the optimum pose was selected for comparison. Calculations were run and images were generated with Flare™, version 9.0, Cresset®, Litlington, Cambridgeshire, UK.

The best pose for each compound was evaluated based on the obtained dG-scoring function docking scores in addition to visual inspection, taking into account the coordination, hydrogen bond interactions, and hydrophobic contacts compared to those observed for the co-crystallized ligand.

3 Results and discussion

3.1. NSC-dots characterization

More than 70% of the synthesized C-dots had a good quantum yield.[46] The methods described by Dong Y. *et al.* provide a basis for this, as their computed luminescence quantum yield was 73.0% when using quinine sulfate as a reference material activated with 345 nm UV light.[46] Furthermore, using a second standard, 4′,6-diamidino-2-phenylindole (DAPI) dissolved in dimethylsulfoxide, Dong Y. *et al.* assessed the quantum yield of the used NSC-dots and discovered that it was 71.2%.[46] Regarding the stability, the solution exhibited excellent stability, maintaining its original characteristics for a period of almost eight weeks.

The produced NSC dots were characterized utilizing a variety of microscopic and spectroscopic techniques. UV-vis spectroscopy and fluorescence were utilized to determine the optical characteristics of the generated NSC-dots. The luminescence spectrum of the prepared NSC dots was scanned, and as shown in Fig. 1B, it has an emission wavelength at $\lambda_{em} = 418$ nm and an excitation at $\lambda_{ex} = 370$ nm. After the addition of 20 μg mL^{-1} of ICA to the NSC-dots solution, its luminescence was quenched, as illustrated in Fig. 1B. After that, the absorption spectra were captured, as shown in Fig. 1C.

TEM was conducted to visualize the morphology, particle size, and distribution of the NSC dots, providing direct evidence of their structural features. Fig. S1A and S1B in the SI reveal that the synthesized NSC-dots are spherical with particle sizes ranging from 2.18 to 9.8 nm. Moreover, FTIR analysis was performed to identify the functional groups present on the NSC-dots' surface and confirm the chemical bonding characteristics. Fig. S1C in the SI shows that an amino N–H stretching vibration band was observed at 3418 cm^{-1}. A broad absorption band ranging from 3400 cm^{-1} to 2500 cm^{-1} is attributed to the carboxylic hydroxyl O–H stretching vibration. The presence of the sulfhydryl (S–H) group was confirmed by the absorption band at 2578 cm^{-1}. Carbonyl (C=O) stretching vibrations were detected at 1713 cm^{-1} and 1634 cm^{-1}, corresponding to carboxylic acid and amide carbonyl (Amide I), respectively. Finally, the C=N stretching vibration (Amide II band) was assigned to the peak at 1544 cm^{-1}. The NSC-dot characterization information acquired here using TEM, FT-IR, UV-visible spectroscopy, and fluorescence spectroscopy aligns with previous reports.[46–49]

Additionally, an XPS examination was performed to clarify the chemical states and elemental composition of the synthesized NSC-dots, offering insights into the surface chemistry of the material. Following the application of the QDs solution on Si substrates, the sample was prepared for room-temperature drying. The spectra of the samples were recorded with an aluminum anode (Al Kα = 1486.6 eV). As shown in Fig. S2 in the SI, the XPS spectrum proved the presence of carbon (C 1s), nitrogen (N 1s), and oxygen (O 1s), which were in agreement with a previous report.[46,49]

Carbon was found in three separate chemical environments, as shown by the three unique peaks found in the high-resolution C 1s spectra. A signal at 284.38 eV was found to correlate with sp^2 C (C–C or C=C), indicating the graphitic nature of the prepared NSC-dots. Peaks at 285.75 eV and 287.45 eV were assigned to sp^3 C (C–N, C–S, C–O) and C=N/C=O, respectively. The O-1s spectra showed two peaks: a peak for C=O at 531.6 eV and a peak for O–H at 530.46 eV. A single peak at 399.95 eV was visible in the N 1s spectrum, indicating the presence of nitrogen in an imine (C=N) group and most likely a pyridinic nitrogen structure. Finally, the high-resolution S 2p spectra showed two peaks: a C–S bond at 163.25 eV and an –S–H bond at 164.54 eV.

3.2. Quenching mechanism elucidation

The fluorescence intensity of the manufactured NSC-dots was quantitatively quenched upon the addition of increasing concentrations of ICA, as demonstrated in Fig. S3 in the SI. Three major categories can be used to describe the quenching mechanism: dynamic quenching, inner filter effect (IFE), and static quenching.[47,48] IFE was thought to be an analytical error until recently. However, recent analysis has come to acknowledge it as a major quenching mechanism involving an energy conversion that has nothing to do with radiation.[30,47] The drug's absorption spectrum and the excitation spectra of the manufactured NSC-dots were considerably overlapped, as seen in Fig. S4 in the SI, which shows that IFE might be involved in the quenching mechanism.[30,47,48,50]

The corrected fluorescence intensity was computed using the following eqn (3) to investigate the effect of the inner filter:[30,47,48,50]

$$F_{\text{corrected}} = F_{\text{observed}} \times 10^{(A_{\text{ex}}+A_{\text{em}})/2} \quad (3)$$

where $F_{\text{corrected}}$ is the corrected fluorescence intensity after the removal of IFE, F_{observed} is the observed fluorescence intensity, and A_{ex} and A_{em} are the ICA absorbance at the excitation and emission wavelengths of the NSC-dots, respectively.[30,47,48,50]

Next, the suppressed efficiency (% E) for the corrected and observed fluorescence intensities was calculated using the following formula (eqn (4)):[30,47,48,50]

$$\% E = [1 - (F/F_0)] \times 100 \quad (4)$$

where F and F_0 are the emission intensities of the ICA–NSC-dots admixture and standalone NSC-dots, respectively. A plot of % E *versus* ICA concentration was constructed in Fig. S5 in the SI.[30,47,48,50]

Results in Fig. S5 in the SI demonstrated a decline in the suppression efficacy, indicating that IFE contributes to the ICA-induced quenching of NSC-dots fluorescence.[30,47,48,50]

In addition to IFE, other potential mechanisms that could be involved in quenching the native fluorescence of NSC-dots were identified using the Stern–Volmer eqn (5):[3–6]

$$F_0/F = 1 + K_{\text{sv}}[\text{ICA}] = 1 + K_{\text{q}}t_0[\text{ICA}] \quad (5)$$

where F_0 and F stand for the fluorescence intensities in the absence and presence of the quencher, respectively, K_{sv} represents the Stern–Volmer quenching constant, and [ICA] is the quencher molar concentration. K_{q} represents the bimolecular quenching rate constant, while the average lifetime (10^{-8} s) is symbolized by t_0, and [ICA] is the drug molar concentration.[3,5]

The Stern–Volmer plot's temperature dependency was examined to distinguish between static and dynamic quenching.[3–6] When dynamic quenching occurs, the K_{sv} value rises with temperature; when static quenching occurs, the K_{sv} value falls with temperature.[3–6]

Collisional quenching is brought on by higher temperatures because diffusion proceeds more quickly. However, static quenching is usually less successful because weakly bound complexes dissolve at higher temperatures.[3,4] Four distinct ICA concentrations were measured at three different temperatures (300, 313, and 318 K), and the resulting Stern–Volmer plots were compared (Fig. S6 in the SI).

As can be seen in Fig. S6 in the SI, the increase in temperature leads to a K_{sv} constant decrease. Calculated K_{sv} values were 10.1×10^3, 8.3×10^3, 8.1×10^3 L mol^{-1} at 300, 313, and 318 K, respectively.[3,5]

Therefore, it was concluded that the static quenching mechanism was found to be also responsible for the NSC-dots fluorescence intensity quenching in the presence of the quencher drug.[3,5]

3.3. Method optimization

Several factors were studied to get the best quenching impact and the best sensitivity, such as buffer pH, the effect of diluting solvent, and the effect of incubation time. First, for studying the effect of the buffer pH, the universal Britton–Robinson buffer (0.04 M) was used to cover the pH range of 2–12. Fig. S7A (in the SI) shows that the pH does not affect the improvement in the quenching of the NSC-dots by ICA. Second, for studying the impact of the diluting solvent on the fluorescence intensity, different solvents were studied, such as deionized water, 0.1 M H_3PO_4, 0.1 M H_2SO_4, 0.1 M NaOH, methanol, ethanol, isopropyl alcohol, and acetone. Fig. S7B in the SI illustrates that deionized water has the best quenching effect on the NSC-dots. Finally, we studied the impact of the incubation time after adding ICA to NSC-dots at intervals ranging from zero to thirty minutes. Every five minutes, the fluorescence intensity was measured, as illustrated in Fig. S7C in the SI. It was noted that the ICA quenching of NSC-dots was instantaneous and stable for 30 minutes. So, the method was optimized using deionized water without any buffer, and the fluorescence intensity was measured instantly, making the proposed method a straightforward, simple, less expensive, and environmentally friendly approach.

3.4. Validation of the proposed method

The performance of the proposed technique was validated according to the ICH standards.[47,51] Table 1 shows all of the validation parameters.

3.4.1. Linearity and concentration ranges. Using the previously mentioned ideal conditions, drug concentrations in a range of 1–20 μg mL^{-1} were conducted to evaluate the linearity of the suggested method (Fig. S3 in the SI). The linear regression line's good accuracy and precision were demonstrated by its high correlation coefficient value (r squared-values >0.999) and tiny relative standard deviation percentage of the slope (S_b%) (less than 2%). Additionally, the high F value (41 255) and low significant F value (5.49×10^{-11}) show that the experimental point scatter around the regression line is limited. Furthermore, the plotted points are nearly superimposed on the regression line, as evidenced by the low residual standard deviation value ($S_{y/x} = 1.17$), highlighting the strong linearity of the recommended approach (Table 1).

3.4.2. Accuracy and precision. For accuracy and precision, three synthetic mixtures of ICA were analyzed at different concentrations within the linearity range on the same day and on three consecutive days. The low percentage error (% E_r)

Table 1 Validation parameters for the spectrofluorometric method suggested for the determination of ICA

λ emission	418 nm
λ excitation	370 nm
Linearity range	1–20 μg mL^{-1}
Intercept (a)	19.02
Slope (b)	10.57
Standard deviation of the intercept (S_a)	0.77
Standard deviation of the slope (S_b)	0.07
RSD% of the slope (S_b %)	0.66
Correlation coefficient (r)	0.9998
Standard deviation of residuals ($S_{y/x}$)	1.17
LOD (μg mL^{-1})	0.24
LOQ (μg mL^{-1})	0.73

Table 2 Evaluation of the precision and accuracy of the spectrofluorometric method proposed for the determination of ICA

Precision & accuracy	Nominal (μg mL^{-1})	Found (μg mL^{-1}) ± SD[a]	% RSD[b]	% E_r[c]
Intraday	1.00	0.99 ± 0.01	1.01	−1.00
	2.00	2.02 ± 0.03	1.48	1.00
	10.00	9.99 ± 0.10	1.00	−0.10
	20.00	19.97 ± 0.22	1.10	−0.15
Interday	1.00	1.01 ± 0.02	1.98	1.00
	2.00	2.01 ± 0.03	1.49	0.50
	10.00	10.01 ± 0.14	1.40	0.10
	20.00	19.99 ± 0.31	1.55	−0.05

[a] Mean ± standard deviation for three determinations. [b] Relative standard deviation. [c] Percentage relative error.

results, which did not exceed 2%, and the appropriate percentage recovery (% R) values demonstrated the accuracy of the procedure. Furthermore, the methodology's high accuracy and reproducibility for quantifying ICA in bulk powder were demonstrated by the extremely low percentage relative standard deviation (% RSD) values, which were below 2.0% (Table 2).

3.4.3. Detection and quantification limits. Moreover, the limit of detection (LOD) and Limit of quantitation (LOQ) were computed using the subsequent formulas (3.3 $S_{a/b}$ and 10 $S_{a/b}$), respectively, where b is the calibration graph slope and S_a is the y-intercept's standard deviation. The high sensitivity of the devised method was affirmed by the low values of LOD and LOQ (Table 1).

3.4.4. Selectivity. As ICA is mainly used as an aphrodisiac, the quenching effect of the possible concurrently delivered medications was investigated to gauge the selectivity of the developed luminous sensor. For instance, sildenafil and avanafil are used for erectile dysfunction, in addition to dapoxetine, which is used for the treatment of premature ejaculation. Furthermore, the effect of yohimbine as a nutraceutical aphrodisiac on quantum dots was tested. Due to the investigated anticoagulant effect of ICA, the anticoagulant clopidogrel and the antiplatelet aspirin were tested for the quenching possibility against the devised quantum dots. The effect of a blank nano-formula was also examined. All of the aforementioned drugs and blank did not suppress the fluorescence intensity of the luminous probe or interfere with the ICA fluorometric assay.

3.5. Preparation of icariin-incorporated nanocarriers

Although several studies have confirmed the therapeutic potential of ICA, its poor aqueous solubility and weak bioavailability have seriously prohibited novel drug development. Therefore, the development of water-soluble pharmaceutical preparations incorporating ICA is advantageous to give a preferable curative effect.[9] In this study, whey protein nanoparticles as an ideal polymer were selected for the encapsulation of ICA to address the solubility issue. ICA-loaded whey protein nanoparticles were prepared *via* the solvent evaporation method to improve their water solubility. The formulated nanoparticles displayed a nanoparticle size (335.1 nm ± 16.64), high negative zeta potential (−15.9 ± 4.66) (Fig. S8 in the SI), and high entrapment efficiency (95.99%).

3.6. *In vitro* blood hemolysis

Spectrophotometric assessment of the liberated haemoglobin from the damaged RBCs was used for the evaluation of hemolysis in blood samples after interaction with the therapeutic ingredients. The hemolytic impact of the prepared ICA-loaded whey protein nanoparticles on RBCs was monitored. As depicted in Fig. S9 in the SI, ICA-loaded whey protein nanoparticles exhibited minimal hemolytic rate ranging from 0.54%–3% for the lowest and highest checked concentrations, respectively, indicating excellent hemocompatibility as it is constructed from naturally derived materials. This minimal hemolytic percent could be assigned to the negative zeta potential value (−15.9 mV), which is thought to avoid interaction with the negative RBCs.[38]

3.7. *In vitro* and *in silico* anticoagulant activity

3.7.1. Anticoagulation potential assay. Various studies demonstrated the antiplatelet and anticoagulant activities of dietary-rich flavonoids, as they are qualified to regulate blood coagulation, platelet aggregation, and fibrinolysis, owing to their action on diverse enzymes and receptors. Thus, it is likely that these could create a significant agent in the protection and therapy remediation of CVDs.[52,53] Among the pharmacologically active flavonoids, ICA is a natural flavonoid that displays a remarkable function in preventing and treating CVDs.[9] The pathway of blood coagulation comprises intrinsic and extrinsic mechanisms. *In vitro* anticoagulant tests could reflect an important section of these mechanisms. The expanded aPTT time emphasized the suppression of the common and/or intrinsic mechanisms, while the expanded PT time emphasized the suppression of the common and/or extrinsic mechanisms.[44] The aPTT and PT tests have initially demonstrated the anticoagulant potential of ICA-loaded whey nanoparticles and whey protein nanoparticles compared to the normal saline and normal plasma. As illustrated in Table 3, the mean PT and aPTT of plasma from normal rats were 13.8 ± 0.2 s and 35.6 ± 1.2 s, respectively. The tested normal saline displayed a non-significant prolonging effect on both PT (13.67 ± 0.21 s) and aPTT (35.80 ± 2.21 s) compared to the normal plasma. However, ICA-loaded whey protein nanoparticles significantly prolonged the PT (19.23 ± 0.42 s) and aPTT (100.27 ± 0.93 s), reflecting the inhibition of the intrinsic and extrinsic coagulation pathways,

Table 3 Effect of icariin-loaded whey protein nanoparticles on the PT and aPTT coagulation time *in vitro*[a]

Test	Compared groups	Mean 1 ± SD	Mean 2 ± SD	Adjusted *P* value
PT in seconds	Normal plasma *vs.* normal saline	13.80 ± 0.20	13.67 ± 0.21	0.9269
	Normal plasma *vs.* whey	13.80 ± 0.20	17.67 ± 0.12	<0.0001
	Normal plasma *vs.* formula	13.80 ± 0.20	19.23 ± 0.42	<0.0001
	Normal saline *vs.* whey	13.67 ± 0.21	17.67 ± 0.12	<0.0001
	Normal saline *vs.* formula	13.67 ± 0.21	19.23 ± 0.42	<0.0001
	Whey *vs.* formula	17.67 ± 0.12	19.23 ± 0.42	0.0004
APTT in seconds	Normal plasma *vs.* normal saline	35.60 ± 1.22	35.80 ± 2.21	0.9981
	Normal plasma *vs.* whey	35.60 ± 1.22	86.20 ± 1.05	<0.0001
	Normal plasma *vs.* formula	35.60 ± 1.22	100.27 ± 0.93	<0.0001
	Normal saline *vs.* whey	35.80 ± 2.21	86.20 ± 1.05	<0.0001
	Normal saline *vs.* formula	35.80 ± 2.21	100.27 ± 0.93	<0.0001
	Whey *vs.* formula	86.20 ± 1.05	100.27 ± 0.93	<0.0001

[a] Statistical significance at $p < 0.05$ by one-way analysis of variance (ANOVA), followed by Tukey's post hoc analysis.

respectively. Surprisingly, the blank whey protein nanoparticles significantly prolonged the clotting time of PT (17.67 ± 0.12 s) and aPTT (86.20 ± 1.05 s) compared to the normal plasma, reflecting the inhibition of the intrinsic and extrinsic coagulation pathways, respectively. The results demonstrated that, among the tested compounds, ICA-loaded whey protein nanoparticles displayed superior anti-coagulant activity *via* expanding the PT and aPTT coagulation times, suggesting that incorporating ICA into whey protein nanoparticles has synergistic impacts against blood coagulation. The good therapeutic performance of whey protein against blood clotting and thrombotic disorders was recently confirmed by Tabassum *et al.*[54] It was concluded that whey protein peptides and amino acids could exert valuable impacts on the vascular performance and thus share roles in CVD risk alleviation.[55]

3.7.2. Docking study of the proposed anticoagulant activity of ICA. To investigate the molecular basis of the measured icariin's anticoagulant activity, we performed docking simulations of icariin against various coagulation factors, including coagulation factors, including Xa, IXa, XIa and XIIa. Crystal structures with co-crystallized ligands were obtained from the Protein Data Bank[56] and prepared using the Flare 9.0.0 (ref. 57) protein preparation wizard. Docking and scoring were performed using Lead Finder[58] as a docking tool implemented in Flare, with the co-crystallized ligand serving as a reference.

The dG-scoring function, docking scores, and visual inspections were used to evaluate the predicted binding poses. Icariin exhibited a favorable docking score and maintained key interactions observed for the co-crystallized ligand when docked into the binding site of human coagulation factor Xa (PDB ID: 1IGQ). However, docking to other coagulation factors resulted in either low scores or unfavorable binding poses.

The docking protocol was validated by redocking the co-crystallized ligand for each protein crystal structure, and the obtained docking poses were checked for reproducing the key interactions observed in the crystal structure, in addition to assessing the pose consistency across multiple runs.

On inspecting the obtained docking poses for the ICA into the binding pocket of Human coagulation factor Xa, one of them (Fig. 2) showed a good fit to the active site and maintained the key hydrophobic and hydrogen bonding interactions expressed by the co-crystallized ligand. The selected docking pose was further minimized in complex with the protein structure in order to optimize the observed initial interactions and to relax the structure to optimize the observed protein ligand interactions. Fortunately, the pose selected for ICA expressed a ΔG docking score of -9.341 kcal mol^{-1}, which was comparable to that observed for the co-crystallized ligand (-12.982 kcal mol^{-1}).

Further analysis for the protein ligand interactions expressed by both the co-crystallized ligand and ICA revealed that two major hydrogen bonding interactions are observed for the co-crystallized ligand (Fig. 3a) with the catalytic binding site of coagulation factor Xa. The first one is the hydrogen bonding interaction with the Gln192 side chain and Cys220, where the sulfonyl group acts as the hydrogen bond acceptor. Similarly, ICA was able to produce hydrogen bonding with the same amino acids (Fig. 3b). In addition, the 2-Aryl ring in the ICA structure maintains arene–arene interactions with the Phe174 side chain expressed by the pyridine ring of the co-crystallized ligand. Moreover, the glucopyranosyl group makes additional hydrogen bonding interactions with Ser195 hydroxyl and with the Asp189 carboxylate group. Additionally, a unique hydrogen bonding interaction was formed with the Arg222 guanidine side chain with the icariin carbonyl and rhamno-pyransoyl hydroxyl. All these additional interactions, besides the two main hydrogen bonding interactions alongside hydrophobic interactions, help to stabilize the binding interactions between icariin and coagulation factor Xa. This binding profile indicates a very promising docking score of ICA with a similar binding mode compared to the co-crystallized inhibitor of coagulation factor Xa.

Conclusively, based on the above-mentioned docking results, ICA displayed an inhibitory impact on the activity of coagulation factor Xa and could extend the aPTT and PT coagulation times. In the clotting cascade, factor *X* is a common pathway for the intrinsic and extrinsic pathways. Thus, suppressing factor *X* hinders insoluble thrombin generation from

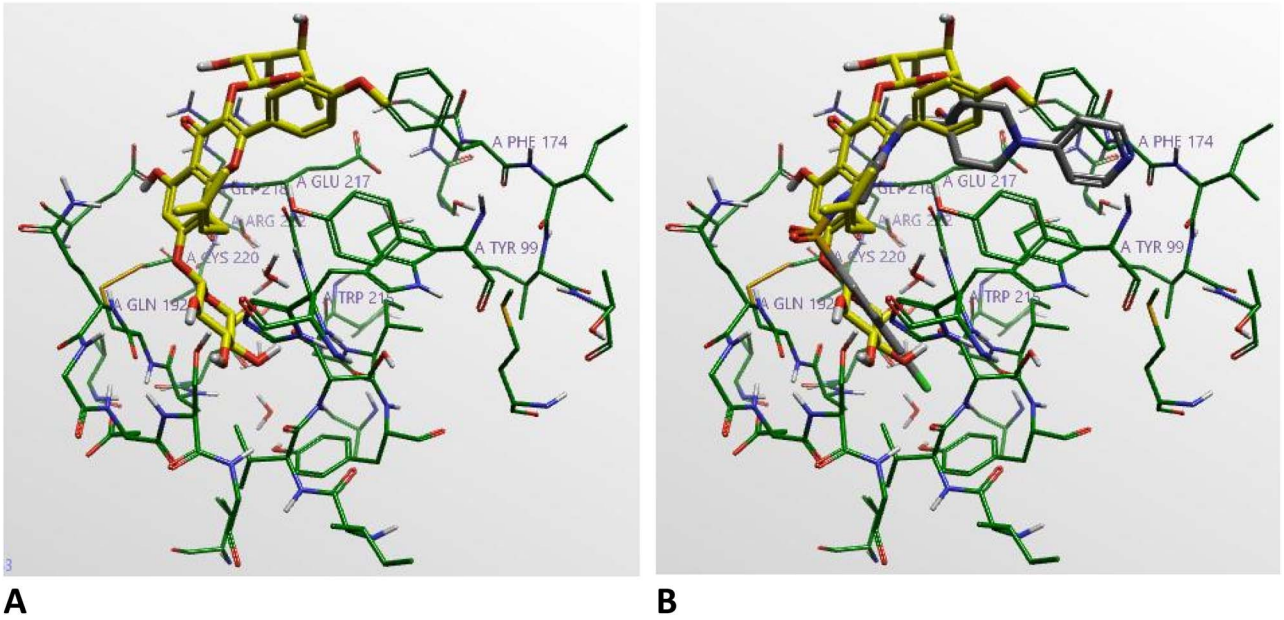

Fig. 2 (A) Selected docking pose for icariin in the catalytic binding site for human coagulation factor Xa (PDB: 1IGQ). Icariin is shown in yellow, while the protein side chains are shown in green. (B) Overlay between the binding pose of icariin (yellow color) and the co-crystallized ligand (gray color).

both pathways.[59] Our results agreed with the results previously published by Bijak *et al.*, who reported on the inhibitory effect of polyphenolic flavonoids on the coagulation factor Xa activity.[60]

3.8. Trio color-coded assessment (green, blue, and white assessment)

The trio color-coded protocol[61–63] provides a comprehensive evaluation of all the steps of the analytical process. It is essential that the analytical technique achieves the Sustainable Development Goals and addresses the environmental safety challenges. Thus, the greenness (ecological), blueness (practicality), and whiteness (sustainability) of the proposed method were extensively compared and evaluated with other reported techniques, such as CZE,[24] HPLC,[25] HPTLC[25] and HPLC-MS/MS.[20]

Different assessment tools were used, including the analytical eco-scale (AES),[64] analytical greenness metric (AGREE)[65] and complex green analytical procedure index (Complex GAPI)[66] for

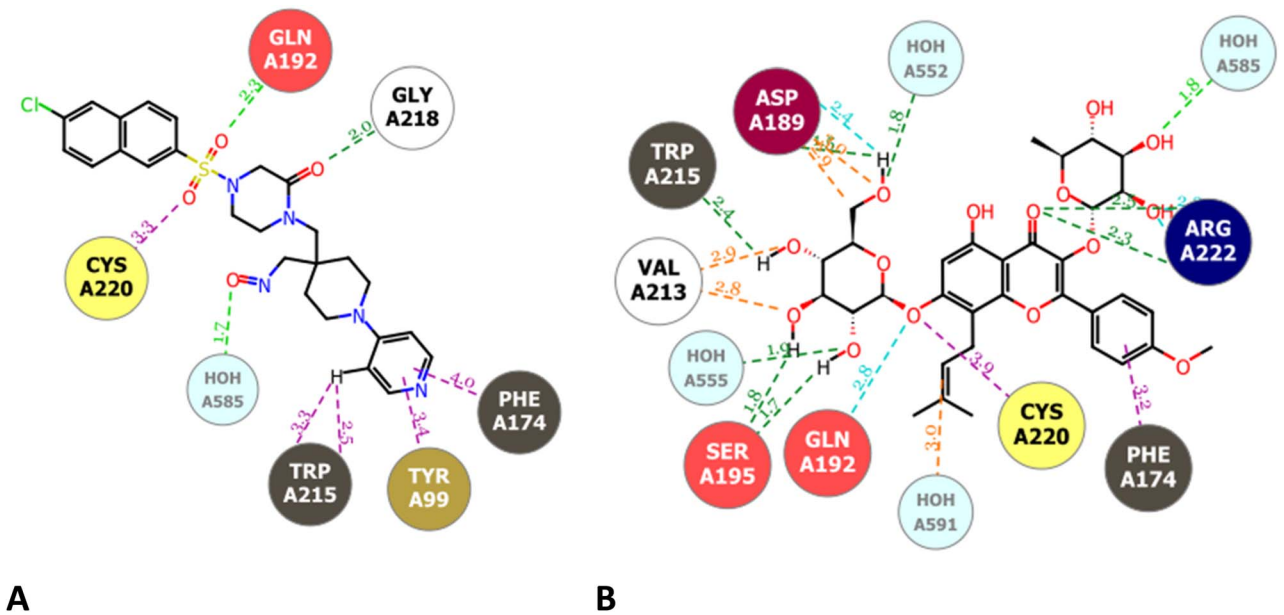

Fig. 3 (A) Binding interactions observed for the co-crystallized ligand. (B) Binding interactions observed for the selected icariin docking pose.

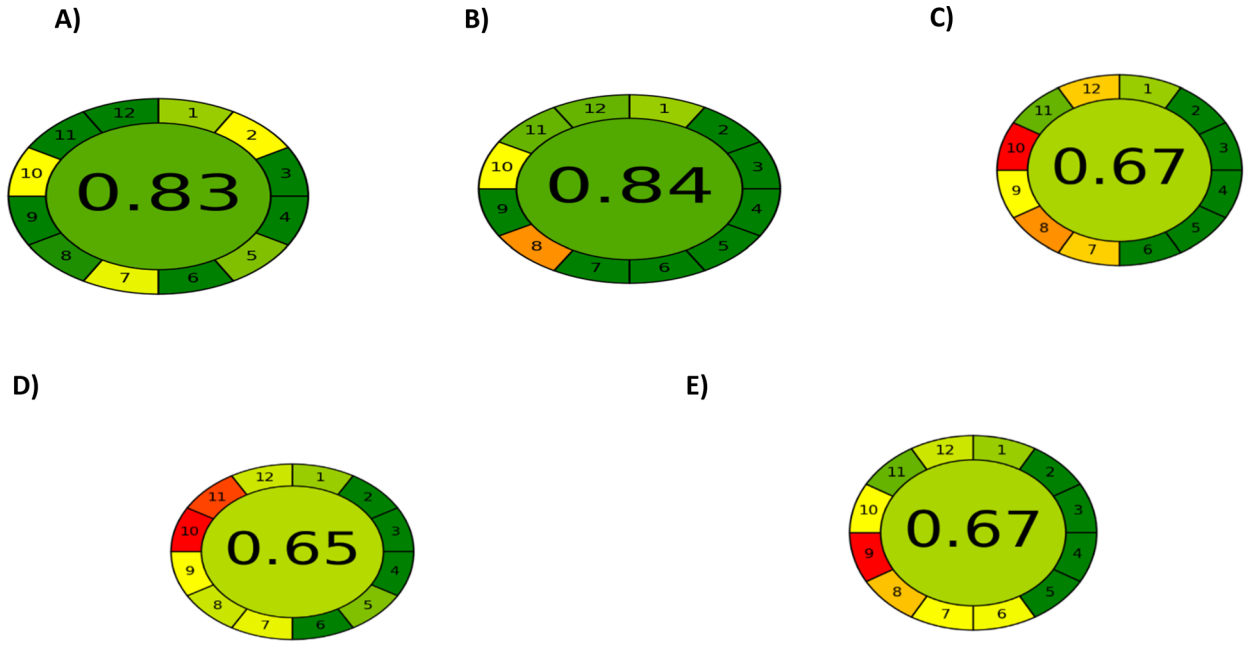

Fig. 4 Comparison of the AGREE of the (a) proposed spectrofluorimetric method with the reported (b) CZE, (c) HPLC, (d) HPTLC and (e) LC-MS/MS methods for the determination of ICA.

the greenness assessment, while the economic and practical aspects were evaluated using the newly developed blue applicability grade index (BAGI).[67] Moreover, the RGB 12 model[68] and RGBfast[69] were implemented to cover all of the attributes of the aforementioned paradigms. These all-inclusive assessment tools evaluated the degrees of greenness or whiteness at different phases, which made the sustainability quotient and environmental impact of the method easy to understand.

With the highest AES score of 94 (above 75) and the highest AGREE result (0.83), the proposed spectrofluorimetric methodology was found to be a superior green analysis when compared with other electrochemical and chromatographic methods (Table S1 in the SI and Fig. 4). This may be attributed to the use of an inert solvent (deionized water) rather than the use of organic solvents (HPLC, CZE, and HPTLC) and derivatizing agents in the case of LC-MS/MS.

Regarding complex GAPI, it is considered an add-on assessment for the well-known green analytical procedure index. It integrates additional fields concerning the process carried out before the main analytical assay. This tool is implemented particularly in cases where the analysis involves the use of deep eutectic solvents or nanoparticles. The devised method shows great performance with 16 green zones and 9 yellow zones, as shown in Fig. 5A. The old GAPI model

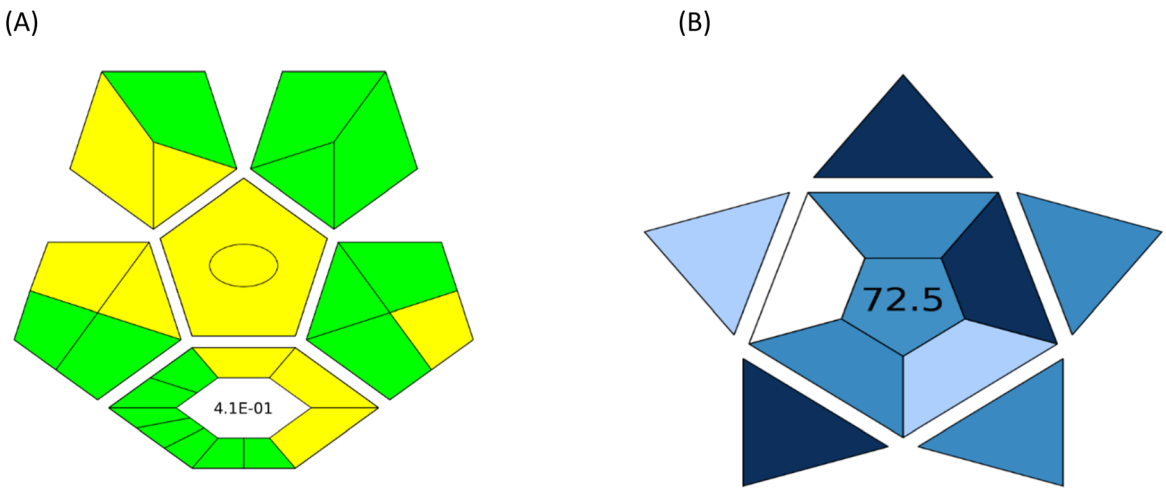

Fig. 5 (A) Complex GAPI diagram and (B) BAGI assessment of the blue profile for assessing the performance of the proposed spectrofluorimetric method for the determination of ICA.

Table 4 RGBfast profiles of the proposed spectrofluorimetric method and other reported methods

Method	Redness	Greenness	Blueness	Whiteness
Proposed spectrofluorimetric method	73.2	81.4	65.5	73
Reported CZE method	50.5	77.2	24.9	46
Reported HPLC method	75.6	37.2	33.2	45
Reported HPTLC method	43.8	69.0	59.6	56
Reported LC-MS/MS method	48.4	33.0	27.5	35

emphasizes the greenness of the spectrofluorimetric assay of ICA, while the extra zones evaluating the synthesis of NSC-dots confirm the ease and greenness of the method. The microwave-driven synthesis mainly used deionized water, and quantum dots could be predominantly used for several assays of ICA.

The novel BAGI software is a new metric to evaluate the applicability and practicality of an analytical procedure. This metric is based on ten main attributes to find the strong and weak points of a method. With a score of 72.5 in the middle of the asteroid pictogram (>60 points), our method is considered practical (Fig. 5B).

The multicriteria RGB-12 model was implemented to acquire a comprehensive assessment of the complete analytical process concerning the GAC's principles, economic factors, and validation criteria.[70–72] As illustrated in Table S2 and Fig. S10 in the supplementary file, our proposed method had the highest blueness score of 95.4, and an acceptable score in terms of redness (93.8) and greenness region (70), and the uppermost arithmetic mean score (whiteness score, 86.4). The explanation for this high score is the usage of deionized water, the low energy consumed by the spectrofluorometer, and the simplicity of the method that has been established. However, alternative

Table 5 Compatibility of the proposed spectrofluorimetric method with various sustainable development goals

SDG	Agreement	Remarks
GOAL 3: good health and well-being	1	Focusing on well-being, this effort uses eco-conscious analytical methods and natural alternatives to address cardiovascular disease
GOAL 4: quality education	1	This research enhances educational quality by providing new insights into the analysis of nutraceuticals, drug repurposing, green chemistry and sustainable practices, enabling their inclusion in teaching and training
GOAL 5: gender equality	1	This project demonstrates fair and balanced involvement from researchers of all genders
GOAL 6: clean water and sanitation	1	This study uses water as a main solvent and actively reduces the waste production
GOAL 7: affordable and clean energy	1	Laboratories can decrease their energy footprint by implementing energy-efficient analytical methods, notably spectrofluorimetric method
GOAL 8: decent work and economic growth	1	A practical method for achieving faster analysis and greater efficiency, resulting in economic benefits
GOAL 9: industry, innovation and infrastructure	1	This versatile analytical technique, applicable to nutraceutical nano-formulations, fosters stronger collaborations between academia and the pharmaceutical sector, leading to substantial time and resource savings
GOAL 11: sustainable cities and communities	1	Ecofriendly practices provide the dual advantage of enhancing urban lab efficiency while minimizing ecological harm
GOAL 12: responsible consumption and production	1	The elimination of dangerous solvents and the reduction of waste in this method translate to a practical and cost-saving solution, leading to reduced time, effort, and expenses
GOAL 13: climate action	1	Environmental safety is paramount in this technique, which uses water and reduces waste, leading to savings in time, money, and labor
GOAL 14: life below water	1	By choosing water as a main solvent, we contribute to the prevention of chemical contamination in water systems, which is vital for marine life
GOAL 15: life on land	1	Shifting to water-based analytical methods, instead of using harmful chemicals, helps to safeguard land-based ecosystems from pollution and damage
GOAL 17: partnerships to achieve the goal	1	Partnerships and collaboration are exemplified by the participation of researchers from multiple disciplines, institutions, and genders, all working towards sustainable scientific practices
Number of agreements	**13**	
% Sustainability	**76**	

techniques such as liquid chromatography need organic solvents and multistep procedures, as well as the high energy consumed by the apparatus and detectors used.

RGBfast is a new version of RGB 12 designed to make assessing whiteness more user-friendly and straightforward. It consists of six assessment criteria with the incorporation of the ChlorTox Scale as a main greenness indicator. As demonstrated in Table 4 and Fig. S11 in the supplementary file, the suggested method had the topmost ChlorTox score (100) and the highest whiteness score (73). As a result, the overall green and white scores are the best.

In summary, the results of the different assessments surpass the performance of the fluorometric approach in comparison to capillary zone electrophoresis (CZE) and liquid chromatographic methods (HPLC, HPTLC, and HPLC-MS/MS). This might be attributed to the use of hazardous organic solvents such as acetonitrile in the case of CZE, HPLC, and LC-MS/MS, while ethyl acetate is used in the case of HPTLC, in addition to the higher cost and energy consumed by the chromatographic techniques. Nevertheless, the suggested method has the advantage of using deionized water as the primary solvent and diluent for everything from QD synthesis to drug analysis. It also offers low-cost, simple, and affordable analysis with no special requirements.

3.8.1. The sustainability proof. While analysts have long recognized the need for green chemistry from the laboratory to industry and have developed various sustainable practices, a crucial link to the United Nations' SDGs has been missing. Analysts are now moving beyond simple 'environmentally friendly' practices by intentionally designing analytical methods to advance these global goals, building on the long-standing understanding of green sustainable chemistry.

To assess the new concept of 'Analytical Chemistry for Sustainability,' a novel evaluation tool, the NQS Index, was developed.[73] This tool combines three critical aspects: 'Need' (based on Koel's pyramids), 'Quality' (using the WAC concept), and 'Sustainability' (aligned with the 17 SDGs), resulting in a single percentage score. Applying this tool to the proposed method yielded the following results: a 'Need' score of 100%, indicating the method's value as a feasible analytical method using a simple sensor; a 'Quality' score of 95%, reflecting its superior WAC profile compared to previously reported analytical methods; and a 'Sustainability' score of 76%, showing alignment with 13 SDGs as illustrated in Table 5. This resulted in an overall NQS Index score (Table S3 in the SI) of 90%, confirming the method's green and sustainable performance.

4 Conclusion and future perspective

The current methodology offers a feasible, valid, cost-effective, and rapid assay of ICA either in bulk form or in whey-based nano-formulation. This spectrofluorimetric framework is based on the quenching tendency of ICA against the in-lab microwave-fabricated quantum dots. Furthermore, a comprehensive investigation of the anticoagulant activity of ICA was performed *in vitro* and *in silico*. Fortunately, the ICA, which is a polyphenolic flavonoid, might have significant activity against Factor Xa, one of the most crucial factors in the coagulation cascade. Thus, this study could be a cornerstone for further biological studies to prove and exploit such activity of ICA. Additionally, the implemented analytical technique, together with its eco-friendliness and sustainability, was assessed and compared with other reported techniques using versatile newly developed metrics. The spectrofluorimetric technique outperformed other alternatives as the devised method depends solely on water as a diluent, in addition to its ease and cost-effectiveness. The method was demonstrated as a trio-colored method (green, white, and blue), in addition to actively pursuing 13 out of 17 of the sustainability goals. Looking ahead, this platform may be extended to other flavonoid-based nutraceuticals supporting broader applications in preventive cardiology and functional food development. Future work may explore *in vivo* validation of the anticoagulant activity, scale-up of the green quantum dot synthesis for industrial applicability, and integration with real-time sensing devices for rapid point-of-care testing.

By integrating green quantum dots in spectrofluorimetric analysis, this approach not only ensures eco-friendly, accurate assessment but also paves the way for more effective and sustainable drug delivery systems in nutraceutical research.

Conflicts of interest

There are no conflicts to declare.

List of abbreviations

AES	Analytical eco-scale
AGREE	Analytical greenness metric
BAGI	Blue applicability grade index
CDs	Carbon dots
CVDs	Cardiovascular diseases
GAPI	Green analytical procedure index
LOD	Limit of detection
LOQ	Limit of quantitation
NSC-dots	Nitrogen sulfur carbon dots
QDs	Quantum dots
RGB	Red green blue

Data availability

The software used for the assessment of greenness and whiteness can be found in the SI of the original papers. AGREE: **https://doi.org/10.1021/acs.analchem.0c01887**. RGB 12: **https://doi.org/10.1016/j.trac.2021.116223**. RGB fast: **https://doi.org/10.1016/j.greeac.2024.100120**. BAGI: **https://doi.org/10.1039/D3GC02347H**. Complex GAPI: **https://doi.org/10.1039/D1GC02318G**. NQS Index: **https://doi.org/10.1016/j.microc.2023.109026**. The software used for the docking study: H. M. Berman, The Protein Data Bank, *Nucleic Acids Res.*, **28**, 2000, 235–242. **https://doi.org/10.1093/nar/28.1.235**. Flare™, version, Cresset®, Litlington, Cambridgeshire, UK;

https://www.cresset-group.com/flare/. Lead Finder™, version, BioMolTech®, Toronto, Ontario, Canada; https://www.cresset-group.com/lead-finder/.

The data supporting this article have been included as part of the SI. Supplementary information is available. See DOI: https://doi.org/10.1039/d5ra04854k.

References

1 M. Bojić, Ž. Maleš, A. Antolić, I. Babić and M. Tomičić, Antithrombotic activity of flavonoids and polyphenols rich plant species, *Acta Pharm.*, 2019, **69**(4), 483–495.

2 B. Subramani and P. Sathiyarajeswaran, Current update on herbal sources of antithrombotic activity-a comprehensive review, *Egypt. J. Intern. Med.*, 2022, **34**(1), 26.

3 P. Pouyfung and S. Sukati, ANTI-COAGULANT PROPERTIES OF FLAVONOID COMPOUNDS: POTENTIAL STRUCTURE-FUNCTIONAL RELATIONSHIP, *Int. J. Appl. Pharm.*, 2021, **13**(1), 9–12.

4 J. P. Quintal Martínez and M. R. Segura Campos, Flavonoids as a therapeutical option for the treatment of thrombotic complications associated with COVID-19, *Phytother. Res.*, 2023, **37**(3), 1092–1114.

5 J. Zhang, D. Xu, Z. Deng, X. Tan, D. Guo, Y. Qiao, Y. Li, X. Hou, S. Wang and J. Zhang, Using tungsten oxide quantum-dot enhanced electrochemiluminescence to measure thrombin activity and screen its inhibitors, *Talanta*, 2024, **267**, 125267.

6 N. Andarwulan, N. Cahyarani Puspita, Saraswati and D. Średnicka-Tober, Antioxidants Such as Flavonoids and Carotenoids in the Diet of Bogor, Indonesia Residents, *Antioxidants*, 2021, **10**(4), 587.

7 K. J. Murphy, K. M. Walker, K. A. Dyer and J. Bryan, Estimation of daily intake of flavonoids and major food sources in middle-aged Australian men and women, *Nutr. Res.*, 2019, **61**, 64–81.

8 C. He, Z. Wang, and J. Shi, Chapter Seven - Pharmacological effects of icariin, in *Advances in Pharmacology*, ed. G. Du, Academic Press, 2020, vol. 87, pp. 179–203.

9 Y. Wang, C. Shang, Y. Zhang, L. Xin, L. Jiao, M. Xiang, Z. Shen, C. Chen, F. Ding, Y. Lu and X. Cui, Regulatory mechanism of icariin in cardiovascular and neurological diseases, *Biomed. Pharmacother.*, 2023, **158**, 114156.

10 Y. Zeng, Y. Xiong, T. Yang, Y. Wang, J. Zeng, S. Zhou, Y. Luo and L. Li, Icariin and its metabolites as potential protective phytochemicals against cardiovascular disease: From effects to molecular mechanisms, *Biomed. Pharmacother.*, 2022, **147**, 112642.

11 Y. Sun, S. Qin, W. Li, Y. Guo, Y. Zhang, L. Meng, Y. Sun, H. Ji, Y. Pan, X. Liu, B. Hu, Y. Shu, Y. Li, Z. Meng, K. Gu, H. Guo, G. Chen, B. Ye, K. Meng and S. PI, A randomized, double-blinded, phase III study of icaritin *versus* huachashu as the first-line therapy in biomarker-enriched HBV-related advanced hepatocellular carcinoma with poor conditions: Interim analysis result, *J. Clin. Oncol.*, 2021, **39**(15_suppl), 4077.

12 D. M. Moss, P. Curley, H. Kinvig, C. Hoskins and A. Owen, The biological challenges and pharmacological opportunities of orally administered nanomedicine delivery, *Expert Rev. Gastroenterol. Hepatol.*, 2018, **12**(3), 223–236.

13 R. Szabó, C. P. Rácz and F. V. Dulf, Bioavailability Improvement Strategies for Icariin and Its Derivates: A Review, *Int. J. Mol. Sci.*, 2022, **23**(14), 7519.

14 H. Z. Asfour, N. A. Alhakamy, U. A. Fahmy, O. A. A. Ahmed, W. Y. Rizg, R. I. Felimban, A. B. Abdel-Naim, M. A. S. Abourehab, R. A. Mansouri, U. M. Omar and S. M. Badr-Eldin, Zein-Stabilized Nanospheres as Nanocarriers for Boosting the Aphrodisiac Activity of Icariin: Response Surface Optimization and *In Vivo* Assessment, *Pharmaceutics*, 2022, **14**(6), 1279.

15 J. Wang, H. Zhu, Y. Jiang, J. Xiao, B. Yang and L. Wen, Fabrication of icariin-soymilk nanoparticles with ultrasound-assisted treatment, *Ultrason. Sonochem.*, 2022, **91**, 106230.

16 Y. Lu, Y. Gao, H. Yang, Y. Hu and X. Li, Nanomedicine-boosting icaritin-based immunotherapy of advanced hepatocellular carcinoma, *Mil. Med. Res.*, 2022, **9**(1), 69.

17 S. Ganguly, P. Das, and S. Margel, Containers for drug delivery, in *Micro-and Nano-Containers for Smart Applications*, Springer, 2022, pp. 127–153.

18 D. C. Polat and M. Coskun, Quantitative Determination by HPLC-DAD of Icariin, Epimedin A, Epimedin B, and Epimedin C in *Epimedium* (Berberidaceae) Species Growing in Turkey, *Nat. Prod. Commun.*, 2016, **11**(11), 1665–1666.

19 O. N. Pozharitskaya, M. V. Karlina, A. N. Shikov, V. M. Kosman, M. N. Makarova and V. G. Makarov, Determination of icariin in rat plasma by reverse-phase high-performance liquid chromatography after oral administration of a lipid-based suspension of *Epimedium* koreanum extract, *Biomed. Chromatogr.*, 2008, **22**(6), 625–629.

20 S. I. Aboras, M. A. Korany, H. H. Abdine and M. A. A. Ragab, HPLC/Fluorescence-Diode Array Detection for Rapid and Reliable Determination of Illegal Synthetic Drugs in Male Sexual Herbal and Honey Remedies: Comparative Study with UFLC–MS, *J. AOAC Int.*, 2022, **105**(5), 1288–1298.

21 Y. Gong, S. C. Yip, S. K. Thamarai, J. Zhang, H. K. Lee and E. L. Yong, Trace analysis of icariin in human serum with dansyl chloride derivatization after oral administration of *Epimedium* decoction by liquid chromatography tandem mass spectrometry, *J. Chromatogr. B:Anal. Technol. Biomed. Life Sci.*, 2007, **860**(2), 166–172.

22 Y. Lu, N. Li, Y. Deng, L. Zhao, X. Guo, F. Li and Z. Xiong, Simultaneous determination of icariin, naringin and osthole in rat plasma by UPLC-MS/MS and its application for pharmacokinetic study after oral administration of Gushudan capsules, *J. Chromatogr. B:Anal. Technol. Biomed. Life Sci.*, 2015, **993–994**, 75–80.

23 J. Liu and Y.-j. Lou, Determination of icariin and metabolites in rat serum by capillary zone electrophoresis: rat pharmacokinetic studies after administration of icariin, *J. Pharm. Biomed. Anal.*, 2004, **36**(2), 365–370.

24 Y. Chai, S. Ji, G. Zhang, Y. Wu, X. Yin, D. Liang and Z. Xu, Determination of icariin in Chinese traditional medicine by capillary zone electrophoresis, *Biomed. Chromatogr.*, 1999, **13**(5), 373–375.
25 O. N. Pozharitskaya, V. M. Kosman, A. N. Shikov, D. V. Demchenko, A. Y. Eschenko and V. G. Makarov, Comparison between HPLC and HPTLC densitometry for the determination of icariin from *Epimedium* koreanum extracts, *J. Sep. Sci.*, 2007, **30**(5), 708–712.
26 G. Somaraj, S. Mathew, T. Abraham, K. G. Ambady, C. Mohan and B. Mathew, Nitrogen and Sulfur Co-Doped Carbon Quantum Dots for Sensing Applications: A Review, *ChemistrySelect*, 2022, **7**(19), e202200473.
27 M. A. Alossaimi, A. S. A. Altamimi, H. Elmansi and G. Magdy, Green synthesized nitrogen-doped carbon quantum dots for the sensitive determination of larotrectinib in biological fluids and dosage forms: Evaluation of method greenness and selectivity, *Spectrochim. Acta, Part A*, 2023, **300**, 122914.
28 S. Miao, K. Liang, J. Zhu, B. Yang, D. Zhao and B. Kong, Hetero-atom-doped carbon dots: Doping strategies, properties and applications, *Nano Today*, 2020, **33**, 100879.
29 G. Magdy, A. A. Al-enna, F. Belal, R. A. El-Domany and A. M. Abdel-Megied, Application of sulfur and nitrogen doped carbon quantum dots as sensitive fluorescent nanosensors for the determination of saxagliptin and gliclazide, *R. Soc. Open Sci.*, 2022, **9**(6), 220285.
30 G. Magdy, S. Ebrahim, F. Belal, R. A. El-Domany and A. M. Abdel-Megied, Sulfur and nitrogen co-doped carbon quantum dots as fluorescent probes for the determination of some pharmaceutically-important nitro compounds, *Sci. Rep.*, 2023, **13**(1), 5502.
31 F. Belal, M. Mabrouk, S. Hammad, H. Ahmed and A. Barseem, Recent Applications of Quantum Dots in Pharmaceutical Analysis, *J. Fluoresc.*, 2024, **34**(1), 119–138.
32 M. Elnaggar, H. Elbardisy, A. El-Yazbi and T. S. Belal, Updated review on carbon dots: their synthesis, characterization and analytical applications, *J. Adv. Pharmaceut. Sci.*, 2024, 42–59.
33 J. Zhang and Y. Zhu, Exploiting the Photo-Physical Properties of Metal Halide Perovskite Nanocrystals for Bioimaging, *ChemBioChem*, 2024, **25**(5), e202300683.
34 S. Chahal, J.-R. Macairan, H.-N. N. Bui, A. Smith, H. C. E. Larsson, R. Naccache and N. Tufenkji, A comparison of carbon dot and CdTe quantum dot toxicity in Drosophila melanogaster, *Environ. Sci.:Adv.*, 2024, **3**(6), 912–924.
35 J. Kong, Y. Wei, F. Zhou, L. Shi, S. Zhao, M. Wan and X. Zhang, Carbon Quantum Dots: Properties, Preparation, and Applications, *Molecules*, 2024, **29**(9), 2002.
36 K. Hayriye Eda Şatana, and E. Nusret, Quantum Dots for Pharmaceutical and Biomedical Analysis, in *Spectroscopic Analyses*, ed. S. Eram, and Z. Fahmina, IntechOpen, Rijeka, 2017, p Ch. 8.
37 M. M. Agwa, D. A. Abdelmonsif, S. N. Khattab and S. Sabra, Self- assembled lactoferrin-conjugated linoleic acid micelles as an orally active targeted nanoplatform for Alzheimer's disease, *Int. J. Biol. Macromol.*, 2020, **162**, 246–261.
38 M. M. Agwa, M. M. Abu-Serie, D. A. Abdelmonsif, N. Moussa, H. Elsayed, S. N. Khattab and S. Sabra, Vitamin D3/phospholipid complex decorated caseinate nanomicelles for targeted delivery of synergistic combination therapy in breast cancer, *Int. J. Pharm.*, 2021, **607**, 120965.
39 M. M. Agwa, S. Sabra, N. A. Atwa, H. A. Dahdooh, R. M. Lithy and H. Elmotasem, Potential of frankincense essential oil-loaded whey protein nanoparticles embedded in frankincense resin as a wound healing film based on green technology, *J. Drug Delivery Sci. Technol.*, 2022, **71**, 103291.
40 M. Agwa, F. E. Elessawy, A. Hussein, M. Eldemellawy, A. Elzoghby, M. El-Salam and A. Eldiwany, Development and validation of an analytical robust method to quantify both Etoposide and Prodigiosin in polymeric nanoparticles by reverse-phase high-performance liquid chromatography, *Anal. Methods*, 2018, **10**, 2272.
41 G. M. El-Sayed, M. M. Agwa, M. T. H. Emam, H. Kandil, A. E. Abdelhamid and S. A. Nour, Utilizing immobilized recombinant serine alkaline protease from Bacillus safensis lab418 in wound healing: Gene cloning, heterologous expression, optimization, and characterization, *Int. J. Biol. Macromol.*, 2024, **270**(Pt 1), 132286.
42 M. M. Agwa, M. R. El-Aassar, R. I. Moustafa, H. Elsayed and N. G. El-Beheri, Rapid RP-HPLC Detection Method For Quantification Of Gentamicin Sulfate Loaded Wound Dressing Nanofiber Formulation With Accelerated *In Vivo* Wound Healing, *Egypt. J. Chem.*, 2024, **67**(6), 445–456.
43 E. I. Amer, S. R. Allam, A. Y. Hassan, E. M. El-Fakharany, M. M. Agwa, S. N. Khattab, E. Sheta and M. H. El-Faham, Can antibody conjugated nanomicelles alter the prospect of antibody targeted therapy against schistosomiasis mansoni?, *PLoS Neglected Trop. Dis.*, 2023, **17**(12), e0011776.
44 S. Xu, F. Fan, H. Liu, S. Cheng, M. Tu and M. Du, Novel Anticoagulant Peptide from Lactoferrin Binding Thrombin at the Active Site and Exosite-I, *J. Agric. Food Chem.*, 2020, **68**(10), 3132–3139.
45 Y. Zhang, G. Wang, Y. Kong, H. Xu, B. Xiao, Y. Liu and H. Zhou, A comparative analysis of the essential oils from two species of garlic seedlings cultivated in China: chemical profile and anticoagulant potential, *Food Funct.*, 2020, **11**(7), 6020–6027.
46 Y. Dong, H. Pang, H. B. Yang, C. Guo, J. Shao, Y. Chi, C. M. Li and T. Yu, Carbon-based dots co-doped with nitrogen and sulfur for high quantum yield and excitation-independent emission, *Angew. Chem., Int. Ed.*, 2013, **52**(30), 7800–7804.
47 M. M. Elnaggar, A. F. El-Yazbi, T. S. Belal and H. M. Elbardisy, White sustainable luminescent determination of nifuroxazide using nitrogen–sulphur co-doped carbon quantum dots nanosensor in bulk and various pharmaceutical matrices, *RSC Adv.*, 2023, **13**(43), 29830–29846.
48 H. M. Elbardisy, M. M. Elnaggar, T. S. Belal, M. A. Ragab and A. F. El-Yazbi, Green "turn-off" luminescent nanosensors for the sensitive determination of desperately fluorescent antibacterial antiviral agent and its metabolite in various matrices, *Sci. Rep.*, 2023, **13**(1), 14131.

49 A. R. Ahmed, H. S. Elbordiny, M. M. Elnaggar, M. A. Ragab, T. S. Belal and S. I. Aboras, Trio-Colored Appraisal of Microwave-Assisted Synthesis of Carbon Quantum Dots as a Fluorescence Turn Off Nanoprobe for Analyzing Ledipasvir in Tablets and Rat Feces: Study of Silymarin Impact on Excretion Recovery, *Luminescence*, 2025, **40**(3), e70138.

50 G. Magdy, E. Aboelkassim, R. A. El-Domany and F. Belal, A novel ultrafast synthesis of N, S-doped carbon quantum dots as a fluorescent nanoprobe for entacapone and clonazepam estimation in tablets and human plasma: Compliance with greenness metrics and content uniformity testing, *Sustainable Chem. Pharm.*, 2024, **38**, 101488.

51 I. ICH, in *Q2 (R1): Validation of Analytical Procedures: Text and Methodology*, International conference on harmonization, Geneva, 2005.

52 B. Olas, J. Żuchowski, B. Lis, B. Skalski, B. Kontek, Ł. Grabarczyk and A. Stochmal, Comparative chemical composition, antioxidant and anticoagulant properties of phenolic fraction (a rich in non-acylated and acylated flavonoids and non-polar compounds) and non-polar fraction from Elaeagnus rhamnoides (L.) A. Nelson fruits, *Food Chem.*, 2018, **247**, 39–45.

53 B. Skalski, B. Kontek, A. Rolnik, B. Olas, A. Stochmal and J. Żuchowski, Anti-Platelet Properties of Phenolic Extracts from the Leaves and Twigs of Elaeagnus rhamnoides (L.) A. Nelson, *Molecules*, 2019, **24**(19), 3620.

54 A. Tabassum, R. Hanumanthappa, K. Jayanna, D. Sannaningaiah and M. Bhagyalakshmi, The Prediction of Milk Whey Extract (MWE) Bioactive Compounds Based on Proximate Analysis and its Effects on Blood Coagulation: A New Approach, *Curr. Res. Nutr. Food Sci. J.*, 2024, **12**, 1.

55 D. Price, K. G. Jackson, J. A. Lovegrove and D. I. Givens, The effects of whey proteins, their peptides and amino acids on vascular function, *Nutr. Bull.*, 2022, **47**(1), 9–26.

56 H. M. Berman, The Protein Data Bank, *Nucleic Acids Res.*, 2000, **28**, 235–242, DOI: **10.1093/nar/28.1.235**.

57 Flare™, version, Cresset®, Litlington, Cambridgeshire, UK, **https://www.cresset-group.com/flare/**.

58 Lead Finder™, version, BioMolTech®, Toronto, Ontario, Canada, **https://www.cresset-group.com/lead-finder/**.

59 K. P. Cabral and J. E. Ansell, The role of factor Xa inhibitors in venous thromboembolism treatment, *Vasc. Health Risk Manage.*, 2015, **11**, 117–123.

60 M. Bijak, M. B. Ponczek and P. Nowak, Polyphenol compounds belonging to flavonoids inhibit activity of coagulation factor X, *Int. J. Biol. Macromol.*, 2014, **65**, 129–135.

61 H. S. Elbordiny, S. M. Elonsy, H. G. Daabees and T. S. Belal, Design of trio-colored validated HPLC method for synchronized multianalyte quantitation of four top selling antihyperlipidemic drugs in different fixed-dose combined tablets, *Green Anal. Chem.*, 2024, **8**, 100100.

62 A. R. Ahmed, S. M. Galal, M. A. Ragab and M. A. Korany, Trichromic sustainable tools of derivative/discrete Fourier transform HPLC convoluted peaks: Application on LCZ696, an antihypertensive supramolecular complex, with its in process and degradation impurity analysis, *Microchem. J.*, 2024, **200**, 110307.

63 S. I. Aboras, A. R. Ahmed, T. S. Belal and H. S. Elbordiny, A tri-hued and sustainable assessment of HPLC for the concurrent determination of multi-purpose binary and ternary vonoprazan combinations: Application to combined dosage forms and simulated gastric juice, *Microchem. J.*, 2025, **213**, 113882.

64 A. Gałuszka, Z. M. Migaszewski, P. Konieczka and J. Namieśnik, Analytical Eco-Scale for assessing the greenness of analytical procedures, *Trends Anal. Chem.*, 2012, **37**, 61–72.

65 F. Pena-Pereira, W. Wojnowski and M. Tobiszewski, AGREE-Analytical GREEnness Metric Approach and Software, *Anal. Chem.*, 2020, **92**(14), 10076–10082.

66 J. Płotka-Wasylka and W. Wojnowski, Complementary green analytical procedure index (ComplexGAPI) and software, *Green Chem.*, 2021, **23**(21), 8657–8665.

67 N. Manousi, W. Wojnowski, J. Płotka-Wasylka and V. Samanidou, Blue applicability grade index (BAGI) and software: a new tool for the evaluation of method practicality, *Green Chem.*, 2023, **25**(19), 7598–7604.

68 P. M. Nowak, R. Wietecha-Posłuszny and J. Pawliszyn, White Analytical Chemistry: An approach to reconcile the principles of Green Analytical Chemistry and functionality, *TrAC, Trends Anal. Chem.*, 2021, **138**, 116223.

69 P. M. Nowak and F. Arduini, RGBfast – A user-friendly version of the Red-Green-Blue model for assessing greenness and whiteness of analytical methods, *Green Anal. Chem.*, 2024, **10**, 100120.

70 H. S. Elbordiny, S. M. Elonsy, H. G. Daabees and T. S. Belal, Sustainable quantitative determination of allopurinol in fixed dose combinations with benzbromarone and thioctic acid by capillary zone electrophoresis and spectrophotometry: validation, greenness and whiteness studies, *Sustainable Chem. Pharm.*, 2022, **27**, 100684.

71 A. R. Ahmed, S. M. Galal, M. A. Korany and M. A. A. Ragab, Multicomponent antihypertensive pharmaceuticals determination with related impurity analysis using MEKC: Whiteness and greenness assessment, *Sustainable Chem. Pharm.*, 2023, **33**, 101066.

72 A. R. Ahmed, M. A. Korany, S. M. Galal and M. A. A. Ragab, Green and white MEKC for determination of different anti-diabetic binary mixtures and their triple-combo pill, *BMC Chem.*, 2023, **17**(1), 86.

73 K. Kiwfo, S. Suteerapataranon, I. D. McKelvie, P. M. Woi, S. D. Kolev, C. Saenjum, G. D. Christian and K. Grudpan, A new need, quality, and sustainability (NQS) index for evaluating chemical analysis procedures using natural reagents, *Microchem. J.*, 2023, **193**, 109026.